ECS Journal of Solid State Science and Technology, **7** (9) P452-P455 (2018)
2162-8769/2018/7(9)/P452/4/$37.00 © The Electrochemical Society

Simultaneously Good Stability and High Speed Based on Oxygen-Doped $Zn_{15}Sb_{85}$ Material

Rui Zhang,[1] Yifeng Hu,[1,2,3,z] Xiaoqin Zhu,[1] Qingqian Chou,[4] and Tianshu Lai[4,z]

[1] *School of Mathematics and Physics, Jiangsu University of Technology, Changzhou 213000, People's Republic of China*
[2] *State Key Laboratory of Silicon Materials, Zhejiang University, Hangzhou 310027, People's Republic of China*
[3] *Key Laboratory of Microelectronic Devices & Integrated Technology, Institute of Microelectronics, Chinese Academy of Sciences, Beijing 100029, People's Republic of China*
[4] *State-Key Laboratory of Optoelectronic Materials and Technology, School of Physics, Sun Yat-Sen University, Guangzhou 510275, People's Republic of China*

In this study, the amorphous-to-crystalline transitions of oxygen-doped $Zn_{15}Sb_{85}$ materials were investigated by in situ film resistance measurements. After oxygen doping, the thermal stability, resistance and bandgap of the $Zn_{15}Sb_{85}$ material increased significantly. The data retention temperature for 10 years increased from 58°C of pure $Zn_{15}Sb_{85}$ to 200°C of oxygen-doped $Zn_{15}Sb_{85}$. The X-ray diffraction pattern showed that lots of Sb phases existed in O-doped $Zn_{15}Sb_{85}$, which induced the fast phase change. The formation of some Zn and Sb oxides were confirmed by X-ray photoelectron spectroscopy. The surface morphology observed by atomic force microscopy demonstrated that oxygen doping refined the grain size and restrained the crystallization. An ultra-short switching time of 2.40 ns was achieved for oxygen-doped $Zn_{15}Sb_{85}$ material. The results showed that appropriate oxygen doping could improve the performance of the $Zn_{15}Sb_{85}$ material in phase change memory.
© 2018 The Electrochemical Society. [DOI: 10.1149/2.0071809jss]

Manuscript submitted June 7, 2018; revised manuscript received August 3, 2018. Published August 11, 2018.

Nowadays, with the current main-stream flash memory approaching its physical limit, a lot of nonvolatile memories have been proposed in the world.[1–3] In these emerging candidates, phase change random access memory (PCRAM) is regarded as the post-flash memory because of its better superiority in ultrafast speed, low power, good endurance, high scalability and multilevel storage. At the same time, the PCRAM is compatible with the manufacture of complementary metal oxide semiconductor (CMOS) processes.[4] In PCRAM devices, data storage is realized by electrical pulse induced reversible phase transition between high resistivity state (amorphous state) and low resistivity state (crystalline state). The significant difference in resistivity between the two states can be used as two different logical states for data storage in PCRAM devices.[5]

$Ge_2Sb_2Te_5$ (GST) is one of the most widely used phase change materials because of its existing business application in optical storage.[6] However, the poor data retention (85°C for 10 years) and slow switching speed in SET and RESET operation processes limit its application in future mass storage. It is reported that the PCRAM device based on GST material is difficult to have an entire operating window when the width of the voltage pulse is shorter than 100 ns, which is insufficient to meet the requirement of dynamic random access memory (DRAM) (∼10 ns).[7] Recently, oxygen doping has been proved to be a useful and convenient way to improve thermal stability by hindering crystallization and reducing consumption, such as O-doped GeTe,[8] Sb_2Te_3[9] and Ge_8Sb_{92}.[10] Sb-rich $Zn_{15}Sb_{85}$ alloy is a phase change material which has an ultrafast phase switching speed due to its growth dominated crystallization mechanism.[11] In this work, oxygen-doped $Zn_{15}Sb_{85}$ materials were prepared. By analyzing the thermal and electrical characterizations, the potential application of PCRAM were evaluated.[12]

Experimental

The O-doped $Zn_{15}Sb_{85}$ materials were prepared by means of magnetron sputtering. The O concentration was under the control of the oxygen flow rate. The total flow rate was fixed at 30 SCCM (Standard Cubic Centimeter per Minute). Through the preliminary screening of experimental data, we selected five samples for further study with the oxygen flow rate of 0, 0.5, 1.0, 1.2 and 1.5 SCCM. The symbols of ZS and ZSOx (x = 0.5, 1, 1.2, 1.5) were used to represent the undoped and O-doped $Zn_{15}Sb_{85}$ materials with the oxygen gas flow of x SCCM, respectively. Then, ZSOx materials were deposited by reactive sputtering of the $Zn_{15}Sb_{85}$ target in an Ar-O_2 gas mixture. The power for the sputtering was fixed at 30 W, with the working pressure for Ar 0.4 Pa. The substrate for material deposition was SiO_2 (300 nm)/Si. The purity of $Zn_{15}Sb_{85}$ target was 99.999% and the thickness of films were 50 nm controlled by sputtering time.

The samples temperature was measured by a Pt-100 thermocouple located at a heating stage controlled by a TP 94 temperature controller (Linkam Scientific Instruments Ltd, Surrey, UK). Thermal stability of amorphous materials was evaluated by isothermal time-dependent resistance measurements. A near infrared spectroscopy (NIR) (7100CRT, XINMAO, China) was used to measure the optical bandgap. The phase structure was investigated by X-ray diffraction (XRD) (X'Pert Pro, Holland) operated at 40 kV and 40 mA using a Cu-Kα source with the 2θ degrees range from 20° to 60°. The binding states of the components were examined by X-ray photoelectron spectroscopy (XPS) (Thermo ESCALAB 250XI, America). The atomic force microscopy (AFM, FM-Nanoview 1000, China) was used to observe the surface morphology of films. The real-time reflectivity was measured by a picosecond laser pump-probe system (EKSPLA PL2143B, Lithuania). The light source used for irradiating the samples was a frequency-doubled model-locked neodymium yttrium aluminum garnet laser with the operating wave-length 532 nm and pulse duration 30 ps.

Results and Discussion

Fig. 1 showed the *R-T* curves of ZS and ZSO_X materials at a constant heating rate of 20°C/min. From Fig. 1, it could be seen that the resistance decreased slowly with the temperature elevating from the start. Then the resistance dropped rapidly to a low and stable value, indicating the transition of amorphous to crystalline state. The temperature at which the resistance has a significant drop is defined as the crystallization temperature (T_c). Before the T_c, the resistance decrease was reversible. When the temperature reached the T_c, the resistance dropped rapidly to a low and stable value which indicated the transition of amorphous to crystalline state. As shown in Fig. 1, the T_c of ZS, ZS0.5, ZSO1.0, ZSO1.2 and ZSO1.5 were ∼145, ∼155, ∼182, ∼218 and ∼240°C, respectively. The thermal stability of metastable amorphous state depended a lot on the T_c. It was clear that the injection of more oxygen atoms improved the thermal stability. Besides, no obvious crystallization process was observed in the ZSO2 material when the temperature increased to 280°C. It could be speculated that the excessive oxygen doping would form too many oxides, resulting

[z]E-mail: hyf@jsut.edu.cn; pacram@jsut.edu.cn

Downloaded on 2018-09-04 to IP 131.204.73.184 address. Redistribution subject to ECS terms of use (see ecsdl.org/site/terms_use) unless CC License in place (see abstract).

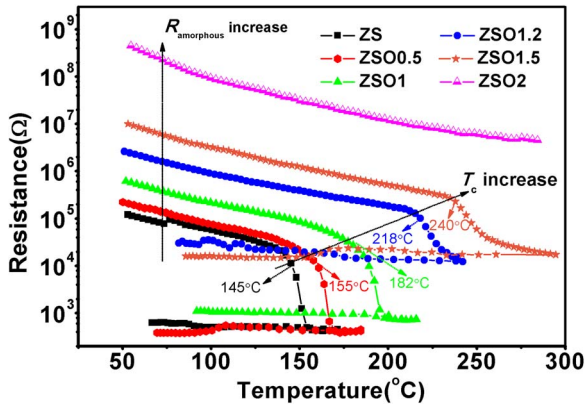

Figure 1. The temperature dependence of resistance for ZS, ZS.5, ZSO1, ZSO1.2 and ZSO1.5, ZSO2 materials at a heating rate of 20°C/min.

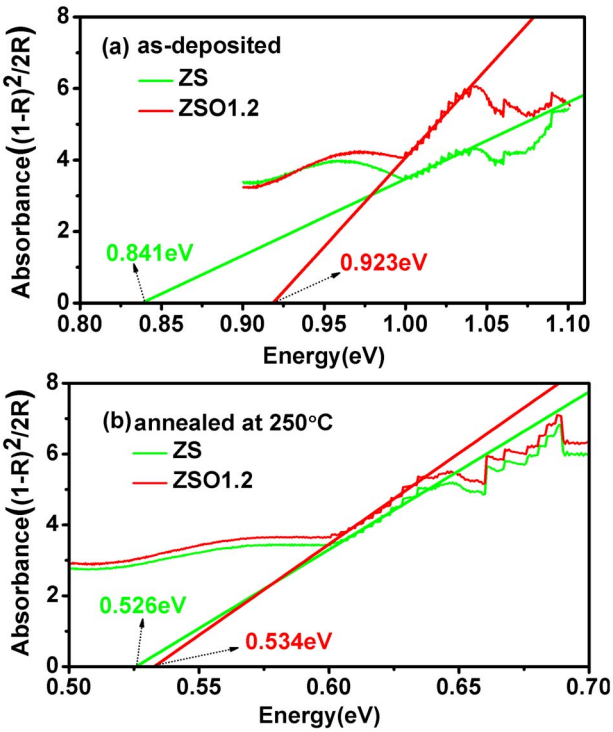

Figure 2. The Kubelka–Munk function of ZS and ZSO1.2 materials: (a) as-deposited ZS and ZSO1.2 material; (b) annealed ZS and ZSO1.2 material at 250°C.

in preventing the crystallization. The amorphous resistances of ZS, ZSO0.5, ZSO1.0, ZSO1.2, ZSO1.5 were 1.3×10^5, 2.1×10^5, 6.2×10^5, 2.5×10^6 and 1.1×10^7 Ω, respectively. The crystallization resistance also increased from 3.75×10^2 Ω of ZS to 1.83×10^4 Ω of ZSO1.5. According to the joule heat $Q = I^2 \times R \times t$, a higher crystallization resistance could improve the heating efficiency and decrease the power consumption.[13] Therefore, we could conclude that ZSO0.5, ZS5O1.0, ZSO1.2 and ZSO1.5 material had lower SET and RESET power consumption than ZS. Also, the resistance difference for ZSOx materials between amorphous and crystalline state was more than one order of magnitude, which could meet the application for PCRAM.

The bandgap energy (E_g) could be determined by extrapolating the absorption edge onto the energy axis, as shown in the Fig. 2. Where in the conversion of the reflectivity to absorbance data was obtained by the Kubelka-Munk function (K-M):[14]

$$K/S = (1 - R)^2/(2R) \quad [1]$$

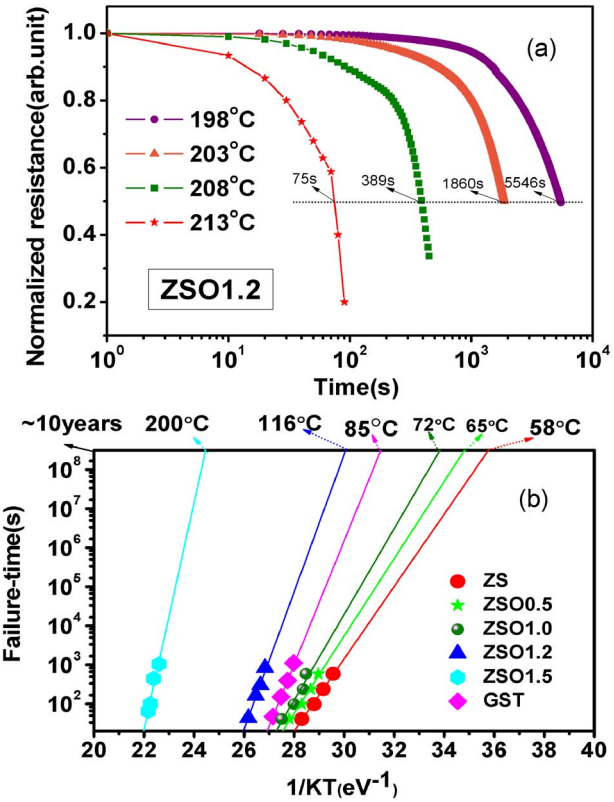

Figure 3. (a) The Kissinger plots of $ln[(dT/dt)/T_c^2]$ vs. $1/T_c$ for the ZSO1.2 thin film. (b) Relationship between logarithm failure time and reciprocal temperature of oxygen-doped ZS and GST materials.

Where R was the reflectivity, K was the absorption coefficient, and S was the scattering coefficient. Fig. 2a showed that the bandgap energy of amorphous ZS and ZSO1.2 materials were 0.841 and 0.923 eV, respectively. After annealed at 250°C for 15 min, the E_g of crystalline ZS and ZSO1.2 materials decreased to 0.526 and 0.534 eV, respectively. The difference of E_g was related to the carrier concentration. Because the carrier density inside the semiconductors was proportional to $\exp(-\frac{E_g}{2kT})$.[15] A broader bandgap would increase the obstacle of carrier transition, leading to the reduction of carriers. It made a major contribution to the increasing of material resistivity after more O adding. This finding supported the conclusions of resistance curves in Fig. 1.

In order to further assess the thermal stability of phase change materials, the isothermal crystallization was carried out. Fig. 3a showed that the failure time of ZSO1.2 at 213, 208, 203 and 198°C was 75, 389, 1860 and 5546 s, respectively. That is, in a lower isothermal temperature, the phase change material needed more time to accumulate enough energy for crystallization. The plot of logarithm failure time versus $1/k_bT$, exhibited in Fig. 3b, fitted a linear Arrhenius relationship because of its thermal activation nature. The linear relationship was described as follows:[16]

$$t = \tau_0 \exp[E_c/(k_b \times T)] \quad [2]$$

Where t, τ_0, E_c, k_b, and T were failure time, a pre-exponential factor depending on the material's properties, the activation energy, Boltzmann constant and absolute temperature, respectively.[17] The time was defined as the failure time when the resistance dropped to the half of its initial value. The data retention temperature (T_{10}) for 10 years obtained by extending the fitted line could be used to estimate the reliability of phase change materials.[13] The T_{10} of GST, ZS, ZSO0.5, ZSO1.0, ZSO1.2 and ZbSbO1.5 were 85, 58, 65, 72, 116 and 200°C, respectively. By comparing ZSOx and GST, it could be found that the

Downloaded on 2018-09-04 to IP 131.204.73.184 address. Redistribution subject to ECS terms of use (see ecsdl.org/site/terms_use) unless CC License in place (see abstract).

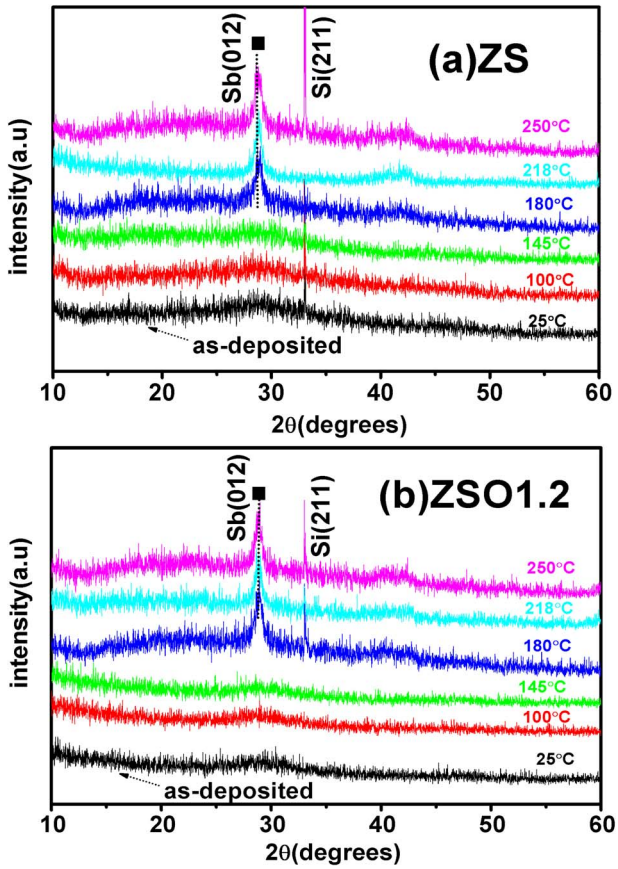

Figure 4. XRD patterns of (a) ZS, (b) ZSO1.2 materials annealed at different temperatures for 15 min in Ar atmosphere.

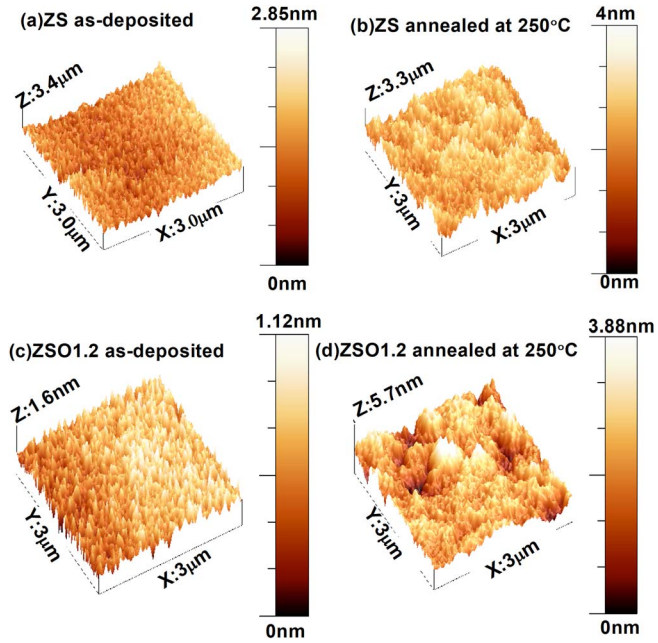

Figure 6. AFM topographic images of (a) as-deposited ZS(500 nm) material; (b) annealed ZS(500 nm) material at 250°C; (c) as-deposited ZSO1.2(500 nm) materials; (d) annealed ZSO1.2 (500nm) materials at 250°C.

T_{10} of ZSO1.2 and ZSO1.5 were higher than GST. That is, O-doped ZS materials could achieve a better thermal stability.

Fig. 4 showed the X-ray diffraction pattern (XRD) of ZS and ZSO1.2 materials annealed at different temperatures for 15 min in Ar gas. There were no diffraction peaks when the annealing temperature was under 145°C, indicating the amorphous structure for ZS and ZSO1.2 materials. Meanwhile, new peak (012) belonging to Sb phase was observed at 180°C, which illustrated the materials began to crystallize. This also manifested the existence of Sb in Sb-rich ZSO1.2 material.[18] No peaks of oxide were observed, indicating that the oxide might exist in amorphous state around the phase change material and inhibited the crystallization.

In order to study the effects of oxygen doping on the changes of chemical composition and bonding state, the XPS measurements were applied for researching ZS and ZSO1.2 materials.[19] As was shown in Fig. 5, the peak of the Zn 2p homopolar bond (Zn-Zn) was at the binding energy of 1021.63 eV for ZS material. After O-doping, the peak shifted to a bigger value (1022.03 eV), indicating that some oxygen atoms have bonded with Zn atoms. In Fig. 5b, the two peaks of the ZS material detected at 527.9 and 537.2 eV corresponded to the Sb 3d5/2 and Sb 3d3/2 peaks of isotope Sb, respectively, which was in accord with the Reference 10. Apparently, the peaks of Sb 3d5/2 and Sb 3d3/2 shifted to higher binding energy position after oxygen doping, speculating the formation of Sb oxide.[20] Fig. 5c showed the fitted curves of Sb 3d5/2 and Sb 3d3/2 in ZSO1.2 material. The binding energy at 527.9 and 537.2 eV could be indexed to a typical Sb-Sb bond, while the binding energy of 530.1 and 539.5 eV for the bond of Sb-O. The electronegativity of O, Zn and Sb elements are 3.5, 1.6 and 1.9, respectively, which meant the O atoms were inclined to bond with Zn and Sb atoms to form the oxide. It was reported that the oxide condensed near grain boundaries and wrapped around the crystal grains, leading to the smaller grain size and a larger amount of grain boundaries.[14]

The surface roughness of the phase-change materials might affect the quality of the electrode-material interface, which was one of the factors influencing device performance. In this work, we

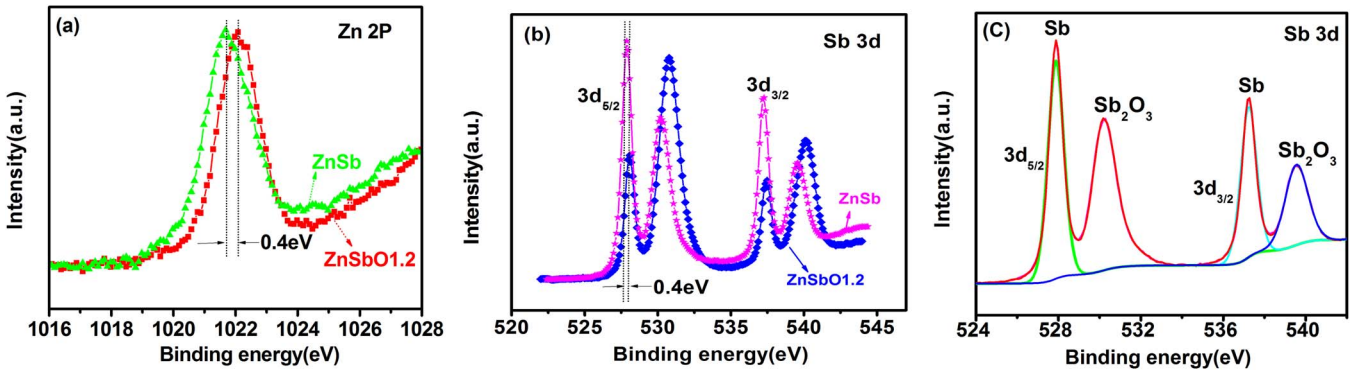

Figure 5. High-resolution XPS spectra of (a) Zn 2*p*3/2, (b) Sb 3*d* for ZS and ZSO1.2 materials. (c) Fitted curves of Sb3d for ZSO1.2 material.

Downloaded on 2018-09-04 to IP 131.204.73.184 address. Redistribution subject to ECS terms of use (see ecsdl.org/site/terms_use) unless CC License in place (see abstract).

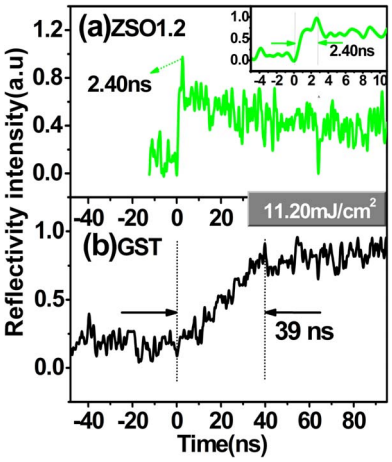

Figure 7. Reflectivity evolution of ZSO1.2 and GST material in the crystallization process: (a) ZSO1.2; (b) GST. The inset in the Figure 7a showed an enlarged view of the data.

selected the as-deposited and annealed samples for comparison. Figs. 6a–6d displayed the AFM images of as-deposited and annealed ZS and ZSO1.2 materials. The root-mean-square (RMS) surface roughness were 0.3106 and 0.1993 nm for as-deposited ZS and ZSO1.2, respectively, which meant the surface was smoother for amorphous films. After annealing at 250°C for 15 min, the roughness of ZS and ZSO1.2 materials increased to 0.4628 and 0.2153 nm, respectively. The results showed that the crystallization was restrained by the adding of oxygen atoms. ZSO1.2 had a smoother surface, which could contribute to the better contact between the electrode and phase change layer.[21]

The phase change speed of materials was a crucial feature because it had a great influence on the switching performance of PCRAM devices. During the phase change, the optical reflectivity also had a great change except the resistivity.[22] The SET operation required lower power than the RESET one, but it needed a longer time. That is, the SET speed and RESET power consumption restricted the speed and power consumption of PCRAM, respectively.[23] The abrupt increase of reflectivity, shown in Fig. 7, was regarded as the amorphous-to-crystalline phase transition. The insets in Fig. 7a showed the magnified figure for the transform of the amorphous-to-crystalline. Fig. 7 showed the crystallization processes for ZSO1.2 and GST material induced by the picosecond laser pulses with the same fluence of 11.2 mJ/cm^2. By comparing Figs. 7a and 7b, we could see that ZSO1.2 material had a shorter switching time of 2.40 ns than that of GST (39 ns). This demonstrated that the phase transition rate of O-doped ZS was faster than GST and a lower power consumption could be achieved if the PCRAM device was based on ZnSbO1.2 material.[24]

Conclusions

In this work, oxygen doping was used to improve the performance of ZS materials. With the increase of oxygen content, the indexes of thermal stability were improved, including the crystallization temperature, data retention for ten years and activation energy (ZS: T_c~145°C, T_{10} ~58°C; ZSO0.5: T_c~155°C, T_{10} ~65°C; ZSO1.0: T_c~182°C, T_{10} ~72°C; ZSO1.2: T_c~218°C, T_{10} ~116°C; ZSO1.5: T_c~240°C, T_{10} ~200°C). After oxygen doping, the bandgap was broadened (amorphous ZS 0.44 eV; ZSO1.2 0.53 eV). The phase structure analysis showed that there were rich Sb phases in the O-doped ZS materials. Some Zn and Sb atoms bonded with O atoms to form oxide to inhibit the crystallization. A small value of surface roughness 0.2153 nm for crystalline ZSO1.2 material was observed. The ZSO1.2 material had an ultrafast phase change speed of 2.40 ns, which was much faster than GST (39 ns). The results showed that the O-doped ZS had good thermal stability and fast phase change speed for PCRAM application.

Acknowledgments

This work was supported by National Natural Science Foundation of China (No. 11774438) and Natural Science Foundation of Jiangsu Province (BK20151172) and sponsored by Qing Lan Project and Postgraduate Research and Practice Innovation Program of Jiangsu Province (SJCX18_1062) and the Opening Project of State Key Laboratory of Silicon Materials (SKL2017-04) and the Opening Project of Key Laboratory of Microelectronic Devices & Integrated Technology, Institute of Microelectronics, Chinese Academy of Sciences and Postgraduate Research.

ORCID

Yifeng Hu https://orcid.org/0000-0001-7088-6829

References

1. H. Zou, Y. F. Hu, X. Q. Zhu, and Z. T. Song, *RSC Advances*. **7**, 31110 (2017).
2. H. Zou, Y. F. Hu, X. Q. Zhu, D. F. Peng, D. F. Chai, X. S. Wang, B. Liu, and D. H. Shen, *J. Mater. Sci. Mater. El*, 11921 (2017).
3. Y. Meng, L. C. Wu, Z. T. Song, M. H. Jiang, Shuai Wen, J. S. Wei, and Y. Wang, *Mater. Lett.*, **201**, 109 (2017).
4. Y. F. Hu, X. Q. Zhu, H. Zou, L. Zheng, S. N. Song, and Z. T. Song, *J. Alloy. Compd.*, **696**, 150 (2017).
5. Y. H. Zheng, Y. Cheng, M. Zhu, X. L. Ji, Q. Wang, S. N. Song, Z. T. Song, W. L. Liu, and S. L. Feng, *Appl. Phys. Lett.*, **108**, 052107 (2016).
6. D. Dimitrov and H. P. D. Shieh, *Mater. Sci. Eng. B-Solid*, **B107**, 107 (2004).
7. P. H. Lee, P. C. Chang, D. S. Chao, J. H. Liang, S. C. Chang, M. J. Tsai, and T. S. Chin, *Thin. Solid. Films.*, **520**, 6636 (2012).
8. L. G. Zhu, Z. Li, J. Zhou, N. H. Miao, and Z. M. Sun, *J. Mater. Chem. C*, **5**, 3592 (2017).
9. Y. You, S. Morioka, S. Kozaki, R. Satoh, and S. Hosaka, *Appl. Surf. Sci.*, **349**, 230 (2015).
10. W. H. Wu, Z. F. He, S. Y. Chen, J. W. Zhai, S. N. Song, and Z. T. Song, *J. Phys. D Appl. Phys.*, **50**, 095602 (2017).
11. E. Palumbo, P. Zuliani, M. Borghi, and R. Annunziata, *Solid State Electron*. **133**, 38 (2017).
12. W. H. Wu, Y. F. Hu, X. Q. Zhu, Y. X. Sui, L. Yuan, L. Zheng, H. Zou, Y. M. Sun, S. N Song, and Z. T Song, *J. Mater. Sci. Mater. El*, **27**, 2183 (2016).
13. Y. You, S. Morioka, S. Kozaki, R. Satoh, and S. Hosaka, *Appl. Surf. Sci.*, **349**, 230 (2015).
14. Y. F. Hu, M. C. Sun, S. N. Song, Z. T. Song, and J. W. Zhai, *J. Alloy. Compd.*, **551**, 551 (2013).
15. R. Golovchak, Y. G. Choi, S. Kozyukhin, Y. Chigirinsky, A. Kovalskiy, P. Xiong-Skiba, J. Trimble, R. Pafchek, and H. Jain, *Appl. Surf. Sci.*, **332**, 533 (2015).
16. W. H. Wu, Y. F. Hu, X. Q. Zhu, Y. X. Sui, J. Z. Xue, L. Yuan, S. N. Song, and Z. T. Song, *J. Mater. Sci. Mater. El.*, **26**, 9700 (2015).
17. J. H. Fu, K. Y. Wang, K. H. Lee, and L. H. Chou, *Thin Solid Films*. **517**, 2813 (2009).
18. H. Peng, L. Xiao Yan, C. Bing, L. Hai Tong, W. Yi Jiao, D. Ye Xin, W. Kang Liang, Z. Lang, G. Bin, D. Gang, Z. Xing, and K. Jin Feng, *IEEE. T. Electron Dev.*, **60**, 4090 (2013).
19. F. Rao, Z. T. Song, Y. Cheng, M. J. Xia, K. Ren, L. C. Wu, B. Liu, and S. L. Feng, *Acta Mater*. **60**, 323 (2012).
20. Q. H. Zheng, Y. X. Wang, and J. Zhu, *J. Phys. D. Appl. Phys.*, **50**, 243002 (2017).
21. Y. Zhang, Jie Feng, and B. C. Cai, *Semicond. Sci. Tech.*, **24**, 045016 (2009).
22. Y. G. Lu, M. Stegmaier, P. Nukala, M. A. Giambra, S. Ferrari, A. Busacca, W. H. P. Pernice, and R. Agarwal, *Nano Lett*. **17**, 150 (2017).
23. H. P. You, Y. F. Hu, X. Q. Zhu, and H. Zou, *J. Mater. Sci. Mater. El.*, **28**, 5562 (2017).
24. J. M. Karanja, P. M. Karimi, W. K. Njoroge, and D. M. Wamwangi, *Thin Solid Films*. **527**, 323 (2013).

Downloaded on 2018-09-04 to IP 131.204.73.184 address. Redistribution subject to ECS terms of use (see ecsdl.org/site/terms_use) unless CC License in place (see abstract).